Morphology of Membranes Formed by the Isothermal Precipitation of Polyamide Solutions from Water/Formic Acid Systems

Chien-Hsueh Shih,[1] Carl C. Gryte,[1] Liao-Ping Cheng[2]

[1]*Department of Chemical Engineering and Applied Chemistry, Columbia University, New York, New York, 10027*
[2]*Department of Chemical and Materials Engineering, Tamkang University, Taipei, Taiwan, Republic of China 25137*

Accepted 3 September 2004
DOI 10.1002/app.21545
Published online in Wiley InterScience (www.interscience.wiley.com).

ABSTRACT: Membranes were prepared by the direct and isothermal immersion of polyamide solutions in a formic acid/water bath. A crystalline polycaprolactam homopolymer, nylon 6, and a largely amorphous terpolymer of nylon 6, nylon 66, and nylon 610 were precipitated from solutions to form complex morphologies on the top and bottom surfaces and cross sections of the membranes. Terpolymer membranes exhibited the characteristics of a liquid–liquid phase-separation process. According to the conditions of the solution and bath, nylon 6 precipitated to form membranes that showed dominance of crystallization or liquid–liquid phase separation. By precipitation from a solution containing a high concentration of a nonsolvent into a bath containing a high concentration of formic acid, skinless nylon 6 microporous membranes were formed. © 2005 Wiley Periodicals, Inc. J Appl Polym Sci 96: 944–960, 2005

Key words: crystallization; membranes; morphology; phase separation; polyamides

INTRODUCTION

The mass transfer of a nonsolvent from a bath into a polymer dope solution will result in the precipitation of polymer into a solid phase, the morphology of which will reflect the precipitation process. The rapid extrusion of a polymer solution into a nonsolvent-rich bath is key to the solution spinning of fibers.[1] If during the solution spinning a continuous gel structure, rather than a dense solid, is formed, exceedingly high-modulus fibers can be prepared by the careful drawing of the gel solid.[2] In contrast to fibers, which are solid, nonporous polymeric threads, semipermeable filtration membranes usually have complex porous morphologies induced by the precipitation of the polymer out of solutions.[3–20] If the bath is a vapor-containing nonsolvent, then the precipitation of an amorphous polymer such as cellulose acetate esters follows the relatively slow dry process to form microporous membranes.[4] Loeb and Sourirajan[5] evaporated the top surface of a polymer solution to accentuate skin formation and then precipitated the polymer by direct immersion in a liquid bath to form a skinned asymmetric cellulose acetate membrane. Such films are highly selective barriers for salt filtration by reverse osmosis. These asymmetric amorphous membrane materials contain a thin surface skin that is supported by an open-cell, phase-inverted, porous substructure that often contains long, finger-shaped macrovoid regions.[6–8] Crystalline polymers have never been very useful as asymmetric membranes for salt-filtration or gas-permeability applications.[9] Marinaccio and Knight[10] and later Pall[11] showed, however, that microporous membrane structures could be made during the precipitation of crystalline polyamides by direct immersion in a nonsolvent. Through the adjustment of the conditions of the precipitation, skinless structures can be formed from many crystalline polymers, which have wide application in separation technologies.[12–20]

Although there is a wealth of art on the subject of making membranes, there is little concrete understanding other than from empiricism of the effects of various elements of membrane preparation on the form and properties of the resultant membranes. Prager et al.,[21] later Smolders and coworkers,[22,23] and more recently Tsay and McHugh[24] and Cheng et al.[25,26] put forward mass-transfer models that track the unsteady-state processes that occur during the immersion of a polymer solution in a nonsolvent. All these models are restricted to events before the formation of a precipitated solid phase. With the exception of some scattered measurements of precipitation times and certain measurements by interferometry,[27] there have

Correspondence to: L.-P. Cheng (lpcheng@mail.tku.edu.tw).
Contract grant sponsor: National Council of Taiwan; contract grant number: NSC 89-2216-E-032-001 (to L.-P. C).

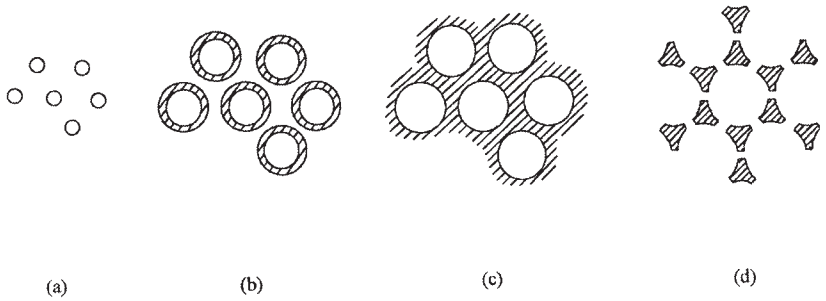

Figure 1 Schematic representation of the stages of the liquid–liquid phase-separation process: (a) nucleation, (b) micelle formation, (c) fusion, and (d) phase inversion.

been no measurements of time-dependent precipitation that offer any possibility of verifying with confidence these computed results. It is the purpose of this report to describe the various events, as deduced from scanning electron microscopy (SEM) photomicrographs of membranes, that are expected during the immersion of nylon 6 in a nonsolvent bath. The solvent/nonsolvent system is formic acid and water. Cheng et al.[25] described a similar precipitation of poly(hexamethylene adipamide). In this work, the sequence of complex nucleation and growth events is organized for the amorphous and crystalline phases, and how the final membrane characteristics depend on both of these precipitation processes is discussed.

THEORY

Types of precipitation processes in aliphatic polyamide systems

Microporous polyamide membranes can be formed by the precipitation of polyamides from various nonsolvent solutions. Depending on the conditions of precipitation (i.e., the conditions of the bath and dope solution), there may be a great variety of precipitated morphologies, each of which may contribute or detract from the ultimate properties of the formed filtration membrane. At one extreme, the precipitated membrane is composed of cellular voids that are surrounded by a polymer matrix. At the other limit, the membrane contains dispersed solid polymer particles surrounded by a continuous void phase. In reality, most precipitation occurs at some intermediate condition in which cellular pores and polymer particles coexist. Because the precipitation of aliphatic polyamides may be induced by crystallization of the polymer and by liquid–liquid phase separation, accounting for the observed precipitate structure is a very complex task. In general, liquid–liquid demixing produces cellular pores, whereas crystallization forms interlinked crystalline elements. The sequence of these two precipitation events dictates the final morphology of the membrane. By a careful inspection of the morphology of membranes of various polyamides (e.g., nylon 6, nylon 66, nylon 610, nylon 12, and Elvamide polyamide terpolymer) prepared by immersion and precipitation from formic acid/water systems, a few types of morphologies that reflect the different relative levels of crystallization and liquid–liquid phase separation have been identified. Although many other morphologies may be encountered, all can be considered intermediate between the following cases.

Case I: Amorphous liquid–liquid phase separation alone

If a largely amorphous polyamide is employed (i.e., a nylon 6, nylon 610, and nylon 66 terpolymer), only liquid–liquid phase separation has to be considered because crystallization occurs merely to an insignificant extent. The liquid–liquid phase-separation process begins with the nucleation of liquid microdrops with compositions close to those of the polymer-poor branch of the binodal, as shown schematically in Figure 1(a). These liquid microdrops (called micelles) are enclosed in a polymer-rich concentration boundary layer, as shown in Figure 1(b), the composition of which is close to that of the polymer-rich binodal. The interface between the micelle and the polymer-rich phase is in equilibrium. The encapsulated micelles grow as a result of diffusional influx of the solvent and nonsolvent from the bulk solution. Radial growth of the micelles occurs and is accompanied by a thickening of the amorphous polymer-rich boundary layers, which enclose the micelles. This process continues until a gelation stage is reached, at which the polymer boundary layers touch, entangle, and then fuse into a homogeneous and continuous polymer gel matrix in which the microdrops (or voids) are dispersed, as shown in Figure 1(c). At this stage, the SEM image of the precipitated terpolymer in Figure 2(a) is observed. If the polymer gel layer is weak and thin, this closed-cell form of the precipitate may undergo phase inversion. As continued densification and shrinkage of the polymer gel occur, the gel boundaries between the

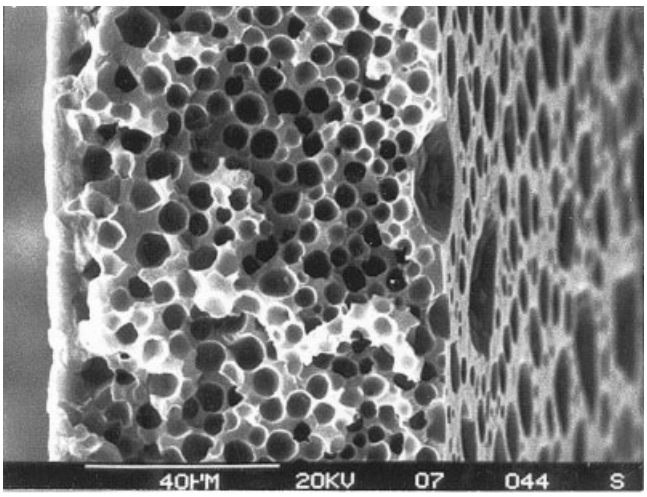

(a)

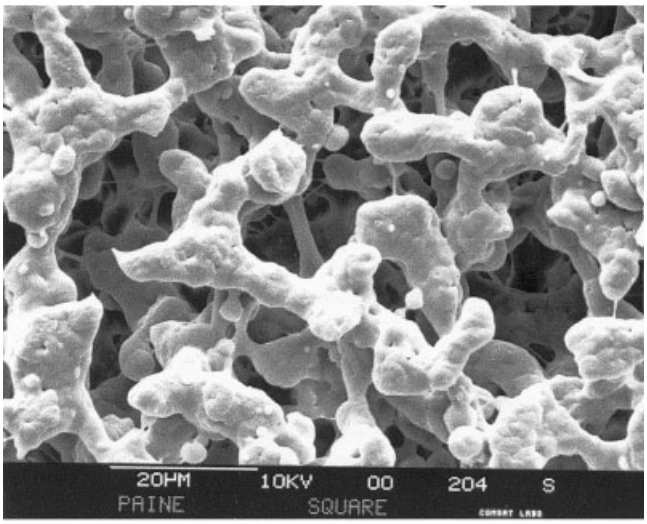

(b)

Figure 2 SEM photomicrographs of terpolymer membranes: (a) 22 wt % terpolymer/1.6 wt % water dope and water bath and (b) made according to Paine.[28]

micellar domains will rupture. The liquid regions will coalesce and become the continuous phase, as shown schematically in Figure 1(d). Ordinarily, a closed-cell structure does not make a useful membrane. However, if a truly open-cell structure can be formed that is uninterrupted from surface to surface, a skinless, porous structure is the result of the precipitation process. In Figure 2(b), an open-cell structure of a terpolymer membrane is illustrated; it is formed during slow vapor-induced precipitation from a terpolymer solution.[28] According to the relative rate of precipitation and gel shrinkage, the micelles may evolve not into spherical regions but into finger-shaped voids. Some publications have reported the possibility of the formation of an open-cell structure (sometimes called a bicontinuous structure) by means of the spinodal decomposition mechanism during an isothermal immersion–precipitation process. For example, Nunes and Inoue[29] and Barth et al.[30] used the light scattering method to show that for membranes precipitated under specific quenching conditions, the light intensity versus the scattering angle could be well fitted to Cahn's spinodal decomposition theory.[31] Kim et al.[32] found from AFM observations that the top surfaces of some membranes exhibited a nodular structure (ca. ~25 nm). These results suggest that spinodal decomposition can act as a phase-separation mechanism in an isothermal process.

The circumstances at the interface (skin region) between the nonsolvent bath and gelling terpolymer must be considered separately from the bulk of the terpolymer discussed previously. The formation mechanism of the skin layer has been described in terms of different separation processes in the literature:[3,17,20,24,33–36] crystallization caused by a sharp concentration increase at the interface, fast precipitation of preexisting small (~20 nm) polymer particles, spinodal decomposition to form nodules at the interface, spinodal composition and then densification by capillary forces in the dry part of the dry–wet process, nucleation and growth to form small polymer-rich spherical domains, vitrification after the interface enters the gelation boundary, and so forth. On the basis of our previous mass-transfer studies, the following interfacial coagulation process for the Elvamide membrane is proposed. Because of the equilibrium boundary condition between the bath and membrane solution, the compositions across this interface lie on the binodal (the ends of a tie line[20–26]). Thus, the interface always contains a polymer-rich boundary region, regardless of what process occurs in the bulk away from the interface. If this polymer gel layer at the interface is stiff, it will survive intact the precipitation beneath it and as a result form a permanent and continuous skin layer. Such a skin is the basis for reverse-osmosis applications. If the skin layer forms under conditions that make it thin and mechanically weak, it can be broken and eliminated by the precipitation process occurring just under it. The result is a skinless structure, and the properties of the membrane depend on the dispersion of precipitated voids in its bulk.

Case II: Liquid–liquid phase separation preceding crystallization

When a crystallizable polymer is precipitated from a solution by a nonsolvent, both liquid–liquid phase separation and crystallization must be considered. The sequences of these precipitation events, which depend on the relative rates of amorphous and crystalline phase nucleation, are known to affect dramatically the resultant membrane morphologies.[15–19,25,26] When liquid–liquid phase separation occurs much earlier than

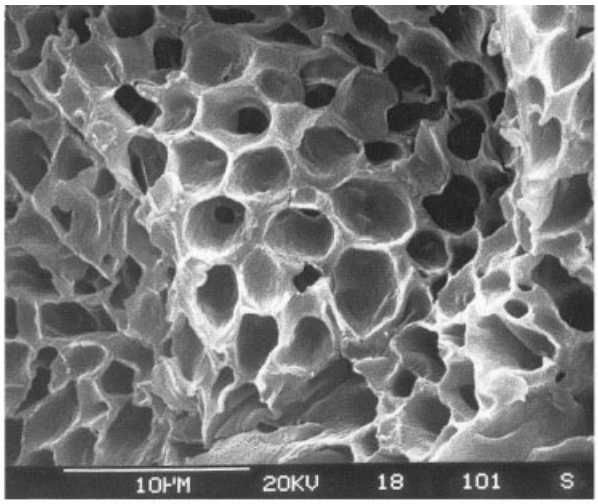

(a)

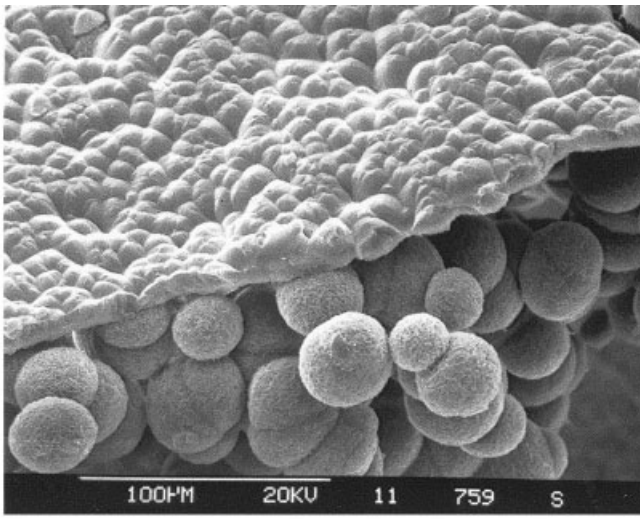

(d)

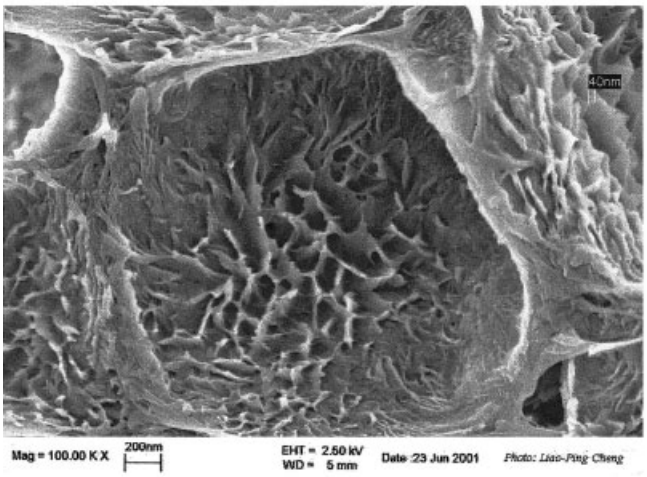

(b)

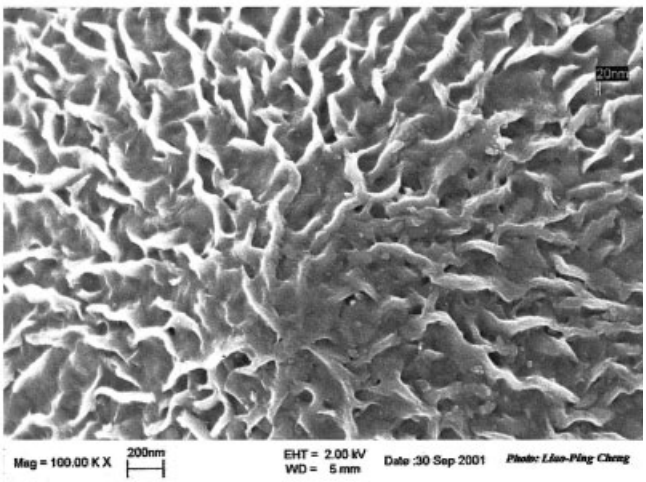

(e)

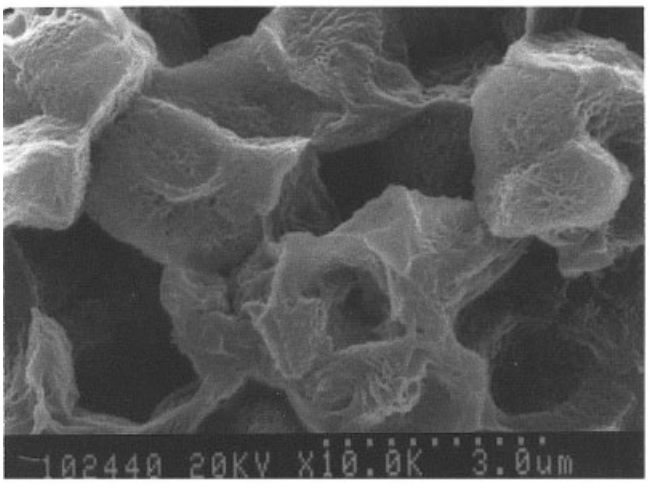

(c)

Figure 3 SEM photomicrographs of various polyamide membranes: (a) nylon 66 membrane cross section (13.1 wt % polymer/1.7 wt % water dope and 29.4 wt % formic acid/water bath), (b) high-magnification micrograph of a cellular pore, (c) nylon 610 membrane cross section (22 wt % polymer/formic acid dope and water bath), (d) nylon 6 membrane top surface (24.7 wt % polymer/1.5 wt % water dope and methanol bath), and (e) high-magnification micrograph of a polygonal unit showing dendrites of polymer crystals.

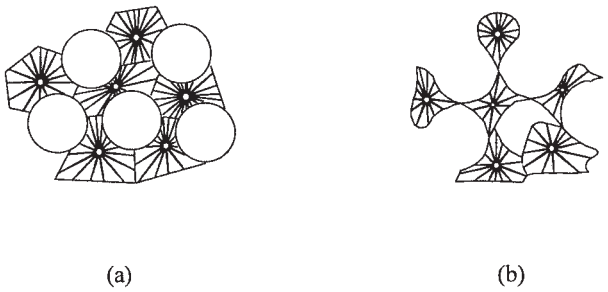

Figure 4 Schematic representation of crystallization after liquid–liquid phase separation: (a) after micelle fusion and (b) after phase-inversion initiation [cf. Fig. 1(d)].

crystallization, the overall membrane morphology is similar to that of the amorphous membrane shown schematically in Figure 1(c), but this membrane will contain spherulitic crystal units on its pore walls. An SEM image of a nylon 66 membrane precipitated into this morphology is shown in Figure 3(a), a high magnification demonstrating the dendritic feature of a pore wall is shown in Figure 3(b), and a schematic representation is given in Figure 4(a). Polymer crystallization in the gel layers that surround the micelles takes place only after the liquid pores are fully developed. In this case, a closed-cell structure forms. Crystallization in the presence of a liquid produces frondlike crystals, which grow on the pore walls in such a way as to produce a rough surface. The overall cellular structure of this membrane is, however, determined by the initially established dispersions of nucleated liquid micelles.

If the crystal nucleation occurs closer to (yet still later than) the time of the liquid–liquid phase-separation events, then the situation illustrated in Figure 3(b) for a nylon 6 membrane is observed. In this case, liquid micelles begin to grow surrounded by a polymer-rich boundary layer. When these micelles begin to aggregate, a nucleation of a crystal phase occurs in the polymer-rich regions. Only a few crystal nuclei are formed in the boundary around each microdrop. These spherulites grow in the polymer-rich gel to form relatively large particles. Their shape, schematically shown in Figure 4(b), is not that expected for a fully grown globular spherulite. The growth pattern is constrained by the shape of the polymer-rich regions that separate the polymer-poor void regions in the film. These growing spherulites continue to reject solvent and nonsolvent from their volume into the micelles, and this further distorts the shape of the voids from that expected in a purely liquid–liquid phase-separated structure. Spherulites may grow in all directions until their fronts meet the adjacent crystallites. As a result, all crystallites in this example are interconnected in the final membrane structure, and because of the low nucleation density, these particles are relatively large. Although distorted, the shape of the voids formed by the initial liquid–liquid phase separation is still evident.

The top surface of the membrane in Figure 3(c) exhibits a skin that is composed of intersecting spherulites in the form of polygonal units.[37] At the top surface layer, at which the equilibrium condition must be satisfied and the local polymer concentration is high,[23,24,26] the nucleation of liquid micelles is inhibited. However, the nucleation of polymer crystallization is highly favored because this layer rapidly becomes supersaturated with respect to crystallization after the immersion of the dope in the bath. Because the polymer does not exist in the bath liquid, the growth of these crystalline particles is confined to the top gel region and leads to the formation of the observed spherulitic polygonal structure. Such top surfaces are not suitable for reverse-osmosis applications because small solutes such as electrolytes are able to leak through the boundaries between adjacent skin spherulites. In Figure 3(c), precipitation under the skin region results in the formation of large, interconnected polymer spherulites. This is discussed later for case IV.

Case III: Crystallization and liquid–liquid phase separation occurring on the same timescale

In case III, liquid–liquid phase separation occurs at approximately the same timescale as crystallization. At some stage when the nucleation of micelles is occurring, as in Figure 1(a), crystal nuclei are also being formed. The bulk morphology in the final precipitate shows evidence of both types of phase-separation processes (i.e., cellular pores from liquid–liquid phase separation and distinct particles from crystallization). Depending on the nucleation density for crystallization, the porous structure varies. For example, for a low nucleation density, the pores are observed surrounded by sheaflike crystalline particles, as shown in Figure 5(a). When the nucleation density is high, the definition of the microdrop voids becomes diffuse and what were the cell walls are now composed of a large number of independent particles, as shown in Figure 5(b). In this case, the liquid micelles grow in an environment filled with growing crystal particles. As a polymer crystal is nucleated, it also generates a boundary layer, which is lean in polymer (the inter-

Figure 5 SEM photomicrographs of various polyamide membranes: (a) nylon 6 membrane bottom surface (22 wt % polymer/15.3 wt % water dope and 39.2 wt % formic acid/water bath), (b) nylon 6 membrane cross section (22 wt % polymer/21.2 wt % water dope and 39.2 wt % formic acid/water bath), (c) nylon 610 membrane cross section, and (d) high magnification of CC.

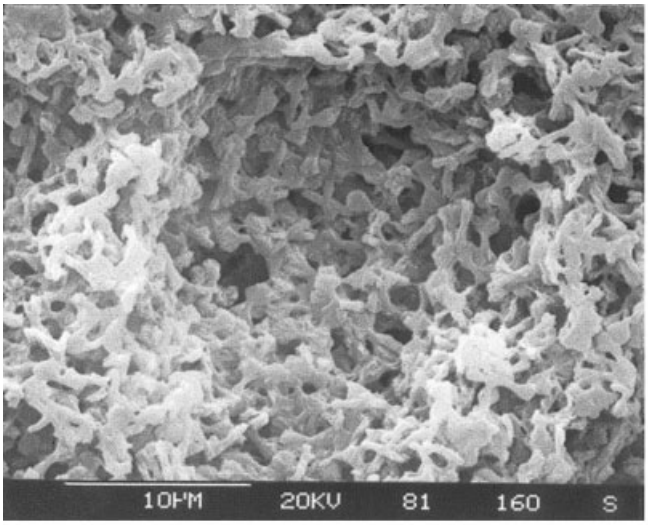

(a)

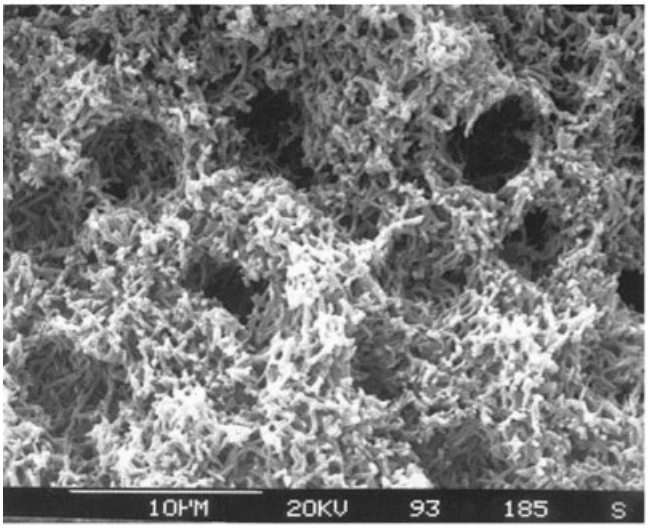

(b)

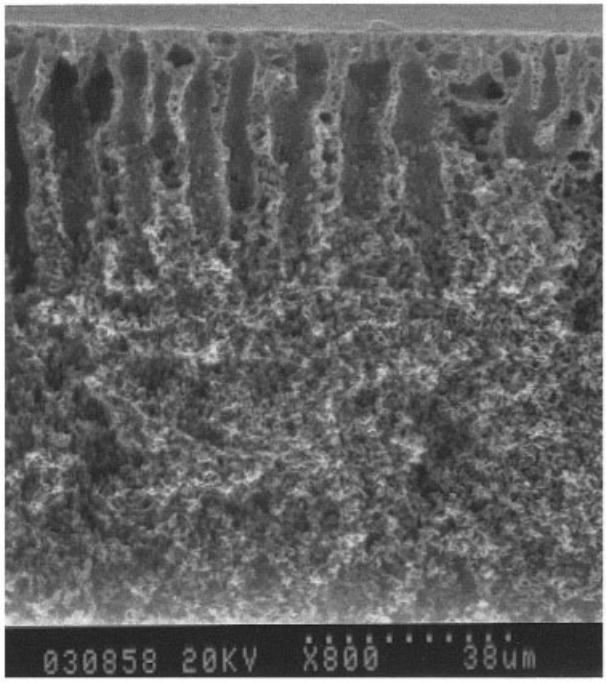

(c)

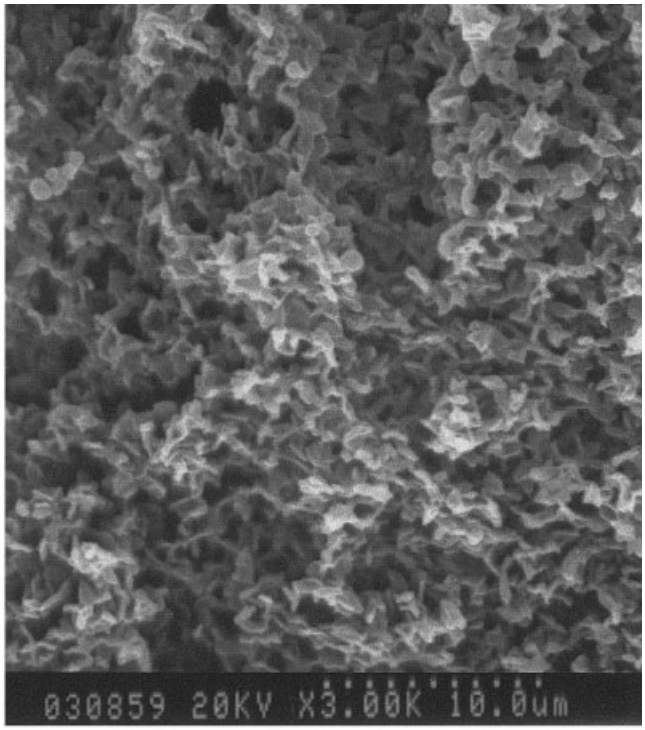

(d)

Figure 5

face is at the equilibrium crystallization boundary condition). This boundary layer separates growing polymeric particles at the early stage of crystallization and inhibits particle–particle interfusion. The particles grow according to the habits of the early stage of spherulite formation. During the growth of crystallites, impurities (solvent and nonsolvent) are expelled into the boundary layer that separates the particles. Finally, the ends of the crystalline particles meet and interlock to form a network.

In some specific precipitation situations, when the composition of the dope is brought close to the binodal, the formed membrane may contain fingerlike macrovoids in its cross section.[38] An example of such a case is shown in Figure 5(c). This structure represents an interesting case in which liquid–liquid phase separation takes place first but crystallization catches up and later dominates the precipitation process. Figure 5(d) demonstrates the high magnification of a macrovoid. Sticklike or sheaflike crystallites are in evidence on the wall of the macrovoid. If crystallization took place before liquid–liquid phase separation during precipitation, nylon 610 would form sticklike or sheaflike crystalline particles distributed uniformly in the entire membrane (see case IV). Furthermore, as crystallization started, it would be impossible for the crystallites to cluster together and reorganize their distribution from within their domains to form macrovoids; that is, the crystalline structure would be fixed in their locations to suppress the tendency of further liquid–liquid phase separation. This suggests that the formation of macrovoids induced by liquid–liquid phase separation occurs first and shortly after this process, and the polymer-rich phase in the vicinity of the macrovoids crystallizes before the vitrification. It is also possible that liquid–liquid demixing and crystallization occur nearly concomitantly. In either case, the formed morphology exhibits features from both liquid–liquid phase separation and crystallization. This is caused by the fact that the dope has a high degree of supersaturation with respect to crystallization, and it is also near the binodal. Thus, the competition between crystallization and liquid–liquid demixing is intense, yielding a membrane with macrovoids originating from liquid–liquid phase separation, and the walls of the latter are composed of crystalline particles.

Case IV: Phase separation occurring by crystallization

Under certain conditions of precipitation, the dopes become supersaturated with respect to crystallization, and so crystal nuclei can form and grow before there is any chance of liquid–liquid phase separation after immersion. Depending on the density of the crystal nuclei, the particles in different membranes will have different sizes and shapes. At low nucleation densities, an array of balls can be observed. The surface of each ball is broken into dendritic structures because of the interfacial instability associated with crystal growth in a very impure environment. Such membranes are weak because the balls are large and the contacts and interlocking between adjacent balls are relatively weak and ineffective. If the nucleation density becomes higher, the spherulites may grow to the sheaf stage. At the highest densities of nucleation, only the preliminary stick stage is reached. The structures of the membranes representing these stages of precipitation are shown in Figure 6(a–c). These were also described by Wunderlich[37] in the context of the stages of spherulitic growth from polymeric melts and were suggested by Smolders[15] to account for the morphology in precipitated nylon 46 membranes. If no skin is formed on the top surface, these membranes are symmetric and microporous. The void regions extend continuously through the cross section. The absence of skin results from the presence of a weak interfacial gel layer that is disrupted by the growing crystalline particles. If conditions are such that a dense skin is formed, the top surface will crystallize into polygonal spherulites, as previously described and shown in Figure 3(c). In some cases, large spherulites grow in the gel region just underneath the boundary between the membrane and precipitation bath. The crystal elements appear as truncated, flattened crystal particles. When nucleation densities are low, each flattened particle may cover a wide area of the membrane surface. If the nucleation density is very high, the flattening of each surface particle is almost impossible to observe, and the membrane appears skinless.

In the discussion that follows concerning the precipitation of nylon 6 in a formic acid/water system, all the aforementioned structural features are observed and are related to the conditions of precipitation.

EXPERIMENTAL

Materials

Polyamides in pellet form were obtained from commercial sources and used as received. Elvamide [8061, DuPont, Wilmington, DE; measured intrinsic viscosity = 1.761 dL/g, viscosity-average molecular weight (M_η) = 56,000 g/mol] is a terpolymer of nylon 6, nylon 66, and nylon 610. Nylon 6 (Zytel 211, DuPont, Wilmington, DE) has an intrinsic viscosity of 1.845 dL/g and a calculated M_η value of 59,000 g/mol. All intrinsic viscosities were measured with an Ubbelohde viscometer at 25°C in an aqueous 90% formic acid solution. The Mark–Houwink constants for the molecular weight calculations were viscosity constant $k = 22.6 \times 10^{-3}$ mL/g and exponent $a = 0.82$ for both nylon 6[39] and the terpolymer. Formic acid (98%; Fluka, Buchs,

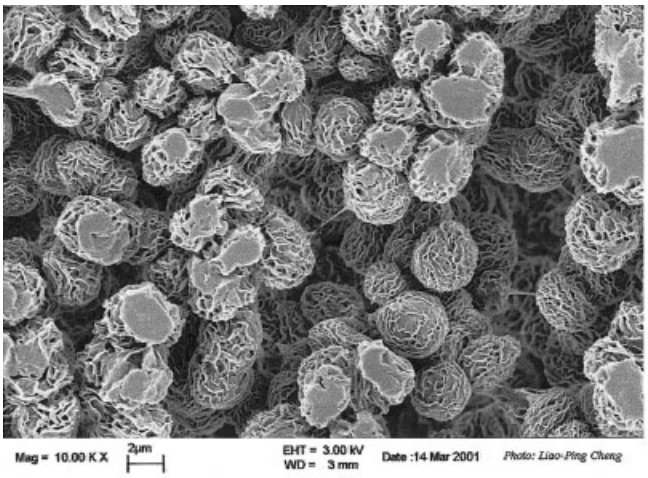

(a)

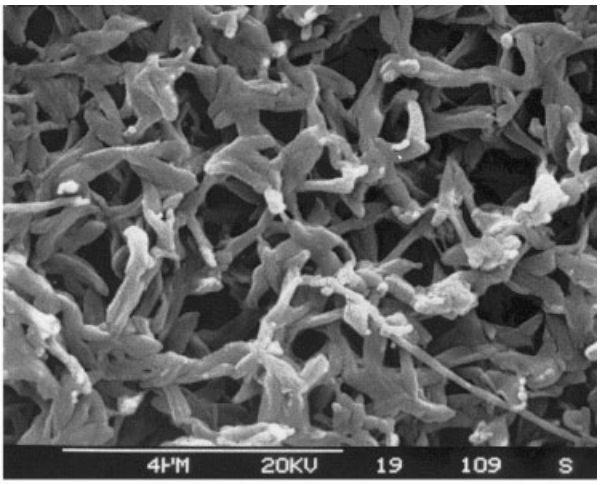

(d)

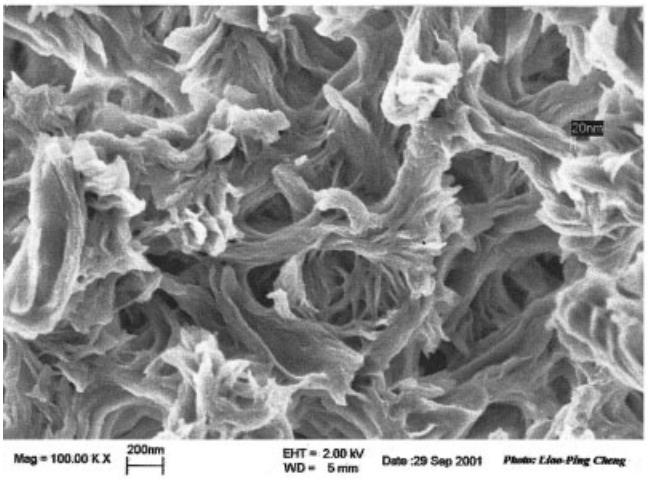

(b)

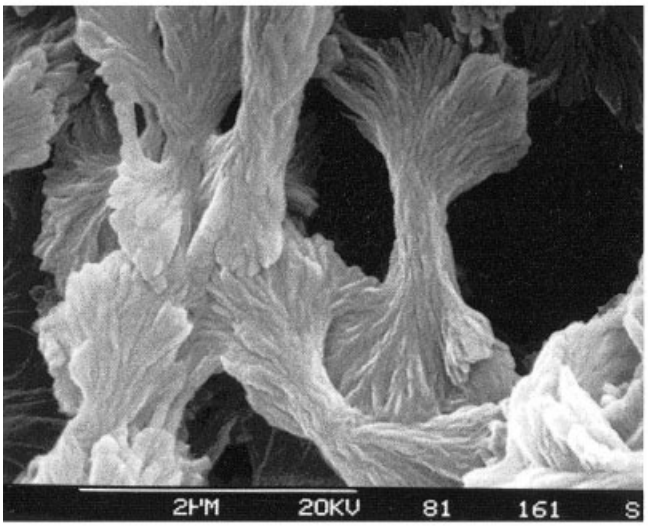

(c)

Figure 6 SEM photomicrographs of various polyamide membranes: (a) nylon 12 membrane top view (5 wt % 1-octanol/75 wt % formic acid/20 wt % polymer dope and 1-propanol bath), (b) nylon 66 membrane cross section (12 wt % water/63 wt % formic acid/25 wt % polymer dope and 10 wt % formic acid/water bath), (c) nylon 6 membrane bottom view (22 wt % polymer/15.3 wt % water dope and 39.2 wt % formic acid/water bath), and (d) nylon 66 membrane cross section (13.1 wt % polymer/18.1 wt % water dope and 29.4 wt % formic acid/water bath).

Switzerland) was used without further treatment. Double-distilled, deionized water was also used.

Membrane preparation and SEM

The procedures have been previous reported in detail.[25] A specific amount of the polyamide (dried in nitrogen at 50°C) was dissolved in a suitable amount of formic acid. To this solution was added a known amount of water and/or a formic acid/water solution to form a dope. Membranes were prepared by the spreading of these dopes on a glass plate and their rapid immersion in a nonsolvent bath. After the precipitation was completed (ca. 20 min), the membranes were removed, rinsed in distilled water, and dried at 45–50°C. The dried membranes were fractured in liquid nitrogen and then coated *in vacuo* with gold palladium. SEM photomicrographs were taken of the top surfaces, bottom surfaces, and cross sections.

Differential scanning calorimetry (DSC) measurements

DSC thermograms for both the terpolymer and nylon 6 were obtained with a TA Q10 thermal analysis instrument (TA Instrument Inc., New Castle, DE) at a heating rate of 10°C/min.

Wettability measurements

The wettability of the membranes was measured with the method described by Pall.[11] A 1 cm × 1 cm piece of a membrane sample was placed on the stage of an optical comparator. A drop of water (2 μL) was deposited on the surface of the film, and the time was recorded for the drop to be completely absorbed. A time less than 5 s implied instantaneous wetting, whereas a time greater than 25 s usually meant the slow absorption of water by the membrane.

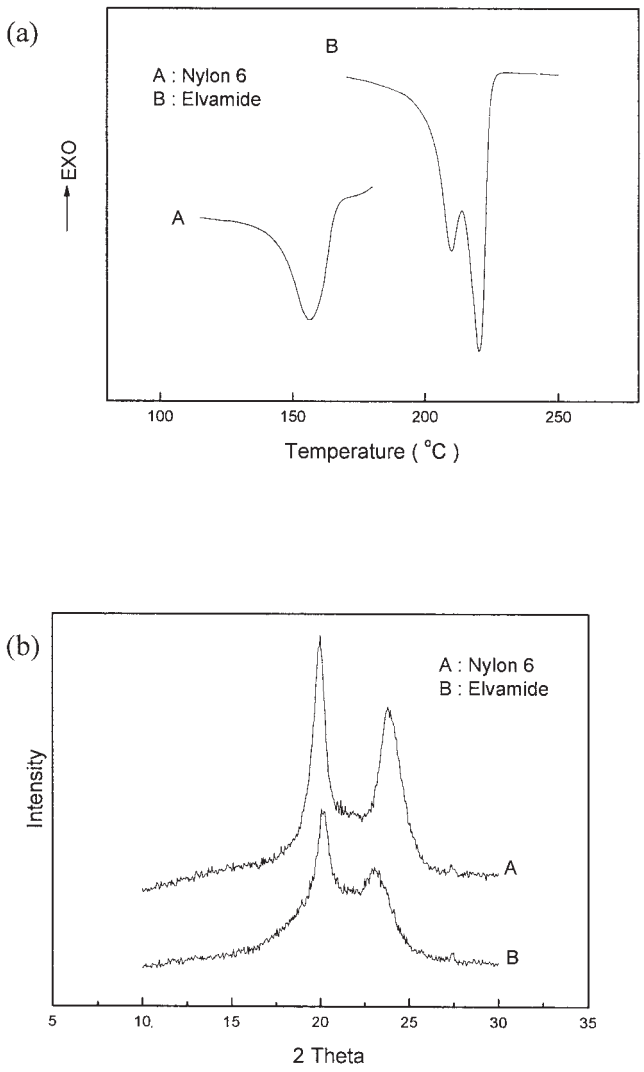

Figure 7 (a) DSC melting endotherms and (b) XRD patterns of polyamide membranes: (A) terpolymer (direct immersion in a water bath) and (B) nylon 6 (direct immersion in a water bath).

RESULTS AND DISCUSSION

Characterization of the membranes by DSC and X-ray analysis

Nylon 6 is a highly crystalline polymer that is soluble in formic acid. Upon the immersion of a casting dope in an aqueous solution, it precipitates into a porous membrane. Thermal analysis by DSC of a typical membrane, as shown in Figure 7(a), indicates a major melting peak (220.5°C) typical of the melting of normal nylon 6 and a less significant peak (209.8°C) at a lower temperature representing the melting of small and less stable crystalline units. In contrast, the terpolymer, which is largely amorphous, shows only a weak and broad melting peak. The DSC thermograms of nylon 6 membranes formed under different precipitation conditions show similar melting behavior but with some variations in the relative magnitudes of the first and second melting peaks. Thus, it can be concluded that although the precipitation leads to different membrane morphologies, the ultimate state of nylon 6 in the membrane is crystalline. Figure 7(b) shows the X-ray diffraction patterns of the terpolymer and the nylon 6 membranes. The nylon 6 membrane exhibits a typical α-type crystal structure.[40] The peaks at 20.66° and around 24° correspond to the reflections of the (200) and (002+202) planes, respectively. The terpolymer membrane also has two peaks. However, they are small and are superimposed on a quite large amorphous halo. These results and those of DSC confirm that Elvamide is largely amorphous yet has some residual crystallinity.

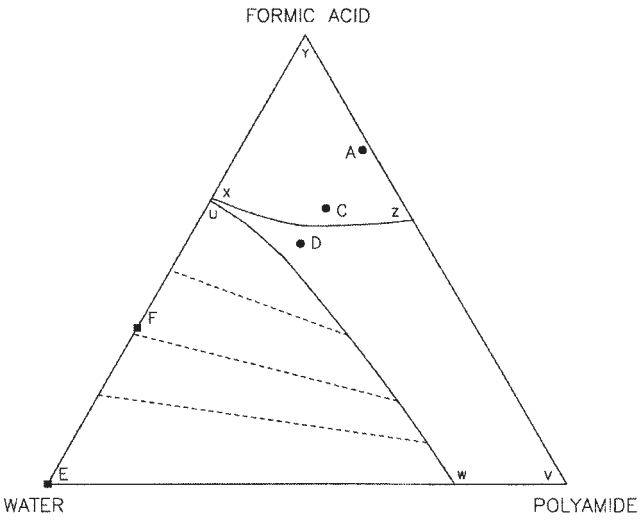

Figure 8 Ternary phase diagram for the water/formic acid/nylon 6 system. The bath compositions were (E) 100 vol % water and (F) 34.6 vol % formic acid, and the dope compositions were (A) 23.9 vol % nylon 6 and 1.8 vol % water, (C) 23.3 vol % nylon 6 and 15.4 vol % water, and (D) 22.3 vol % nylon 6 and 24.3 vol % water.

Phase diagrams, dopes, and baths

The phase diagram for water/formic acid/polyamide at 25°C, determined and reported previously,[41] is shown in Figure 8. There can be identified three important regions, the boundaries being the binodal and the crystallization line. The binodal of nylon 6 has been assumed to approach that of the terpolymer. The justification of this assumption has been reported elsewhere.[41] The region above the crystallization line (area XYZ) is a one-phase region. A mixture in this region is a stable, homogeneous solution that does not undergo any phase separation. The region between the binodal and the crystallization line (area VWUXZ) is supersaturated only with respect to crystallization, and hence the mixture has the tendency to precipitate by polymer crystallization. The region within the binodal (area UWE) is metastable with respect to both liquid–liquid phase separation and crystallization. As a result, both types of phase transformation are anticipated for a dope solution situated in this region. For the largely amorphous terpolymer, precipitation is dominated by liquid–liquid phase separation. Therefore, only the binodal region has to be considered.

Several dope compositions (in the range between points A and D in Fig. 8) and two bath compositions (points E and F in Fig. 8) were used to prepare porous membranes. These dopes were selected because they corresponded approximately to the range of compositions indicated in Knight's U.S. patent[12] for the formation of nylon 6 membranes. Dope A was a homogeneous solution that contained only a small amount of a nonsolvent. As the nonsolvent content was increased in the dopes, the polyamide in dopes C and D was in an increasingly less dissolved state. Dope D was of special interest because it was near the point of incipient precipitation. Although initially clear, this dope became cloudy over an extended period of storage. This effect could be reversed by the heating of the dope to a slightly higher temperature. In this work, only dopes that appeared to be clear at the time of casting were used. It has been pointed out[12,18,19,25] that dopes containing high levels of a nonsolvent may contain polymers in various associated states. These dopes were not true solutions. If a crystalline polymer is dissolved in a medium such that the overall composition is close to the crystalline equilibrium line (XZ in Fig. 8), there will be a very small thermodynamic driving force for the final stages of dissolution. The dissolved polymer may be in some history-defined precrystalline aggregated state that retains some memory of its earlier crystalline condition. Nucleation and growth from such a preaggregated state may be very difficult to reproduce, and it is for this reason that repeatedly making the same membrane from a given formulation often involves a degree of art. Two different types of baths were used in the immersion–precipitation process to make membranes. Bath E (i.e., pure water) was a harsh nonsolvent for the polymer. Upon the immersion of a dope solution in it, the top surface of the membrane was expected to contain high concentrations of the polymer. Such membranes were predisposed to rapid precipitation and skin formation. By contrast, bath F was rather soft and contained a large amount of formic acid (solvent). Because its composition was close to the dope concentration (at least in comparison with the harsh bath), the driving force for mass transfer and consequently the rate of mass transfer and composition change were low. As a result, the driving force for precipitation was lower overall and was spread over a longer period of time.

Amorphous polyamide membrane

In Figure 9(a–c), SEM photomicrographs are shown for a terpolymer membrane prepared by the immersion of dope A into bath F. The cross section [Fig. 9(a)] is characterized by a uniform distribution of spherical pores, which are relatively large in size (ca. 10 μm). The process of precipitation follows case I, which is schematically represented in Figure 1(a–d). Because the crystallinity is rather low for the terpolymer,[40] the cellular pores are formed only by the liquid–liquid phase-separation process. Under these conditions of precipitation, there is no evidence of elongated, fingerlike macrovoids, which are often typical of many polymer precipitating systems.[6–8] Near the upper interfacial region, there is a dense layer about 1–2 μm thick. The top view of this skin layer is shown in Figure 9(b). Unlike the uniform and featureless top

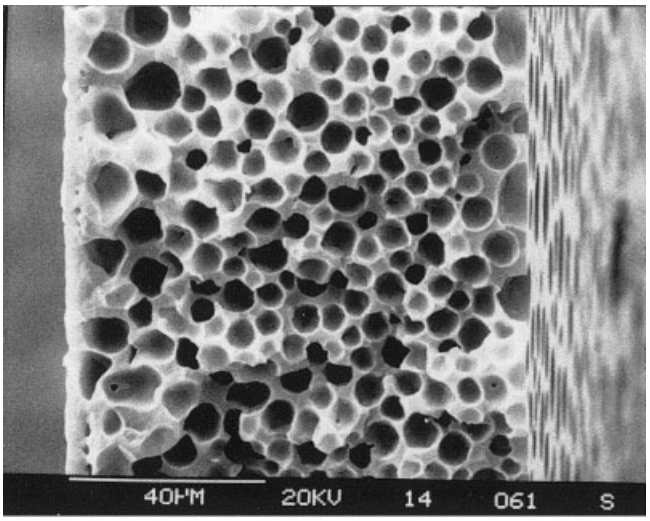

(a)

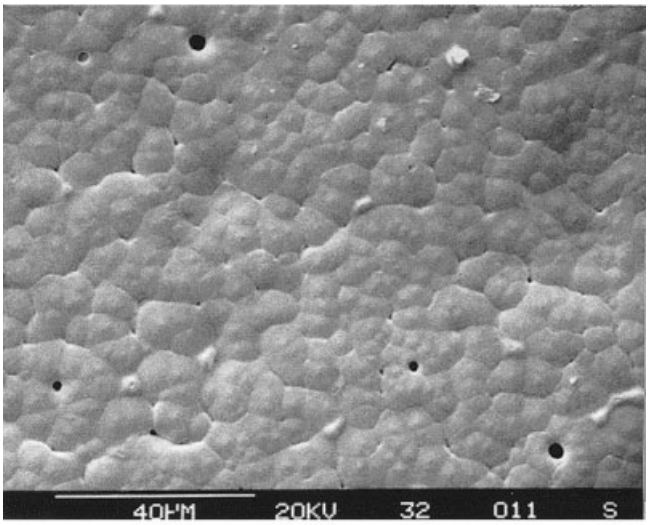

(b)

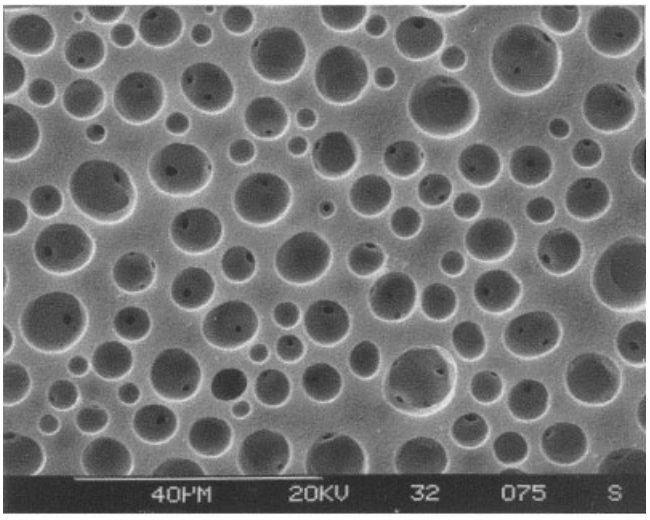

(c)

surfaces for asymmetric membranes of polysulfone or cellulose acetate, which have applications in gas separation or reverse osmosis, this skin contains distinct polygonal features (ca. 5 μm) that have almost linear boundaries. These polygonal areas are similar to the shapes of spherulites that form from crystallization in a subcooled melt under uniform conditions. Between the polygonal grains, the boundaries sometimes show noticeable crevices. A slow spherulitic crystallization of the residual crystalline fraction of the terpolymer may occur within this skin layer in the late stage of the immersion–precipitation process. It is well known that the crystal morphology is discontinuous at grain boundaries because impurities and noncrystalline materials are concentrated in these regions. Thus, the permeability of the surface skin is expected to be a complex function of the grain boundary and bulk polymer porosity. The bottom surface of the membrane shown in Figure 9(c) is typical of terpolymer membranes precipitated under a wide variety of bath and dope conditions. It consists of sharply truncated spherical voids of various sizes. To account for this morphology, a large number of liquid micelles have to nucleate directly on the surface of the glass casting plate (if nucleation occurred exclusively off the glass, a continuous skin would form). These liquid micelles grow into the solution, with one part of their surface being the polymer gel and the other part being the glass surface. Because the wall between the cellular voids is relatively thin, there exists some breakthrough so that some degree of continuity exists between the void regions. However, most cells have the so-called closed-cell structure. Extensive pore–pore interconnection [cf., e.g., Figs. 1(d) and 2(b)] does not occur, and the membrane has very little application for microfiltration.

Effects of the dope conditions on the nylon 6 membrane morphology

The discussion of the effects of the dope composition on the morphology of crystalline nylon 6 membranes is divided into considerations of the cross sections, top surfaces, and bottom surfaces of the membranes.

Cross sections

In Figure 10(a–d), SEM photomicrographs of cross sections are shown for the various dopes (points A, C, and D in Fig. 8) immersed into 40 wt % formic acid/water solutions (bath F). (Hereafter, the membranes

Figure 9 SEM photomicrographs of the terpolymer membrane prepared by the immersion of dope A in water: (a) cross section, (b) top surface, and (c) bottom surface.

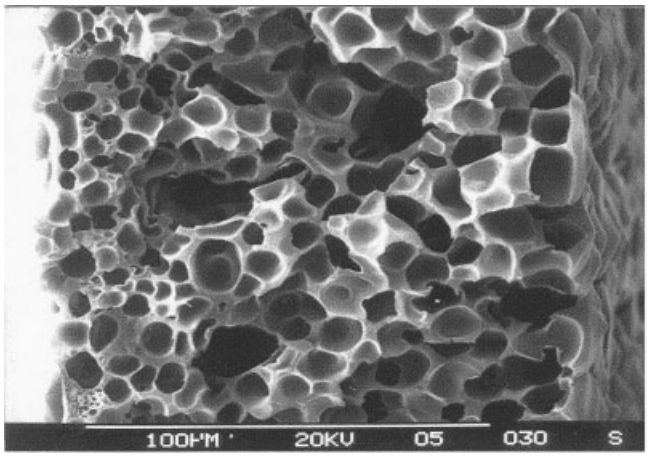

(a)

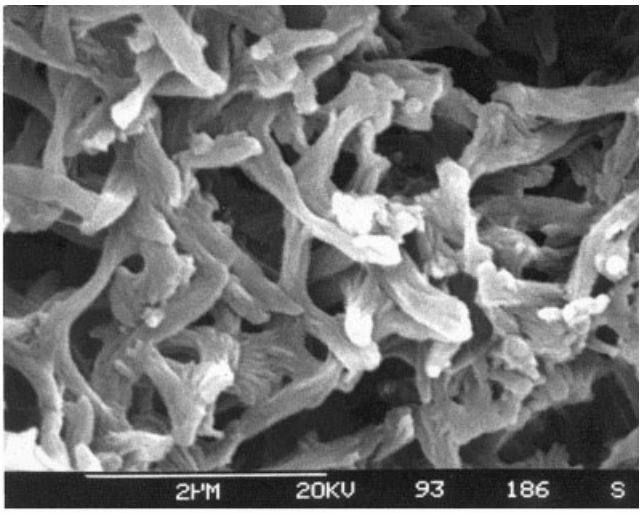

(d)

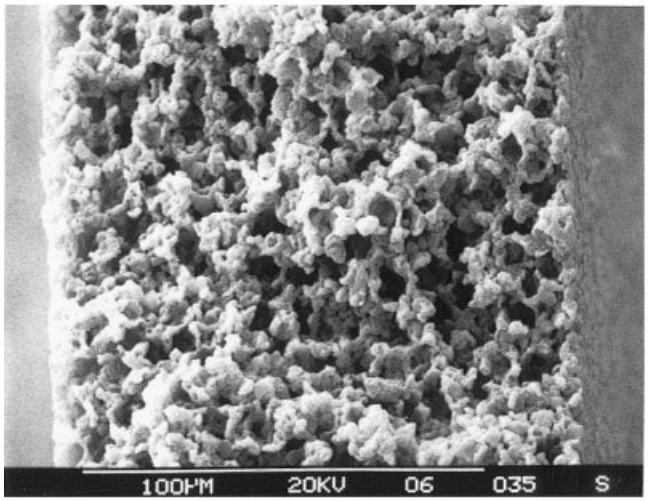

(b)

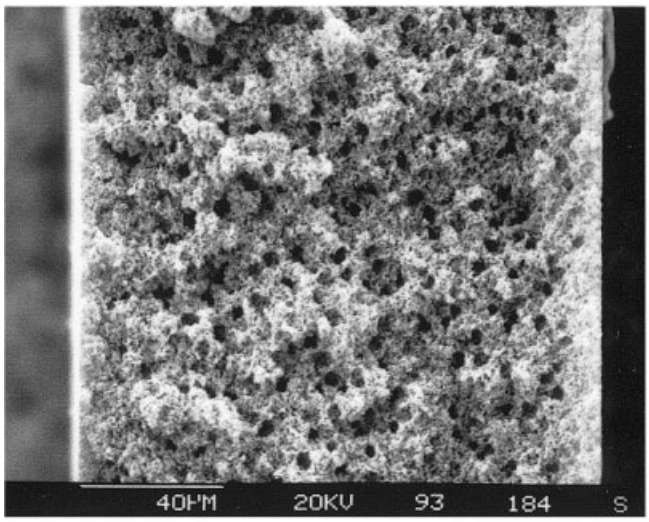

(c)

Figure 10 SEM photomicrographs of cross sections of nylon 6 membranes prepared by the immersion of different dopes in bath F: (a) membrane AF, (b) membrane CF, (c) membrane DF, and (d) membrane DF at a high magnification.

TABLE I
Wettability of Nylon 6 Membranes Precipitated from Water/Formic Acid Solutions

Membrane	Drop absorption time[a]	
	Top surface	Bottom surface
AF	>25	>25
CF	7	7
DF	5	5
AE	>25	>25
CE	>25	>25
DE	>25	>25

[a] A 2-μL drop of distilled water on a 1 cm $\times$ 1 cm membrane sheet.

are named with two letters, the first letter referring to the dope and the second letter to the bath. For example, membrane CE is the membrane prepared by the immersion of dope C into bath E.) Membranes AF, CF, and DF have morphologies that can be described by case II–IV precipitation courses. Apparently, with increasing amounts of water in the dopes (A–D), the relative rate of precipitation by liquid–liquid phase separation and crystallization mechanisms changes. Figure 10(a) indicates that membrane AF has a largely cellular morphology (i.e., case II). Crystallization appears to have only a small effect on the observed overall morphology. This suggests that liquid–liquid phase separation precedes crystallization, and only after the completion of the growth of liquid micelles into cellular pores does crystallization start in the pore walls. The pores are more or less spherical (ca. 12 μm), and there exists only a small level of interconnection between them. The presence of a closed-cell structure reduces significantly the hydraulic permeability of this membrane (Table I). The cross section of membrane CF is shown in Figure 10(b). In comparison with membrane AF, the density of the isolated particles (nylon 6 crystallites) is substantially higher. Such a structure may be classified as intermediate between case II and case III. In this membrane, crystallization and liquid–liquid phase separation appear to occur on the same timescale. Because of the very high population of crystals, the cellular pores are barely distinguishable, and the pore walls are open. In contrast to membrane AF, membrane CF is readily wetted by water, as shown by the wettability test data in Table I. As dope D, which has a composition inside the crystallization equilibrium line XZ in Figure 8, is immersed in soft bath F, a membrane with a skinless, microporous character approaching those membranes developed by Marinaccio and Knight[10] is obtained. The cross section of membrane DF is shown in Figure 10(c), and a high-magnification image is shown in Figure 10(d). A small vestige of a cellular structure (ca. 5 μm) that is attributed to liquid–liquid phase separation can still be observed in Figure 10(c). However, it is certain that this membrane is formed predominantly by crystallization. The membrane pores are constructed by interlocked crystallites in the shape of sticks (ca. 1 μm), which have been identified as an early spherulitic form.[37] This membrane is thus a packed bed of small, interlocking crystallites, and this is consistent with the fact that a microporous membrane with a small pore size must be composed of a matte of very small particles.

Top surfaces

The top surfaces of membranes AF, CF, and DF are shown in Figure 11(a–c). As in the cross-sectional region, evidence of precipitation initiated by crystallization in the top surface increases as the dope composition shifts from membrane AF to membrane DF. The top surface changes from a skin of intersecting polygonal units to an array of independent particulate (skinless) surfaces. Liquid–liquid phase separation does not occur in any of the top gel layers. This layer forms as a result of the mass-transfer boundary condition at the dope solution interface with the bath. Depending on the rate of crystallization in this boundary layer, different morphologies are observed. The polygonal spherulites on the top surface of membrane AF, as discussed earlier, are produced from a highly supersaturated gel of a relatively high local polymer concentration. Its nearly two-dimensional character results because the crystal growth is confined to the gel boundary layer contacting the bath. Each spherulitic grain is quite large (ca. 20 μm). This implies that, in contrast to the typical crystalline bulk of a membrane such as CF or DF [Fig. 10(b–d)], there are relatively few nuclei in the skin region of this nylon 6 membrane. In Figure 11(a), holes can be observed in the top skin surface that are caused by a skin-rupture process[34] that occurs when the formed gel layer is very thin.

When the nucleation density at the top surface becomes considerably higher, as for membrane CF [Fig. 11(b)], the surface becomes virtually skinless, there being little evidence of any remnant of a continuous polymer-rich layer. The crystalline particles (ca. 3 μm) observed in this top surface are large enough to be considered spherulitic sheaves.[37] These crystalline particles are nucleated in the bath–membrane boundary layer, and their growth results in isolated particles rather than a continuous layer. The separation of particles occurs because each particle is surrounded by a polymer-poor boundary layer. This boundary layer prevents particle–particle contact and inhibits the formation of a continuous polycrystalline surface film, such as that seen in the top surface of membrane AF [Fig. 11(a)]. The top surface of membrane DF is shown in Figure 11(c). It is composed of small and sticklike crystalline particles[37] similar in size (ca. 1 μm) and

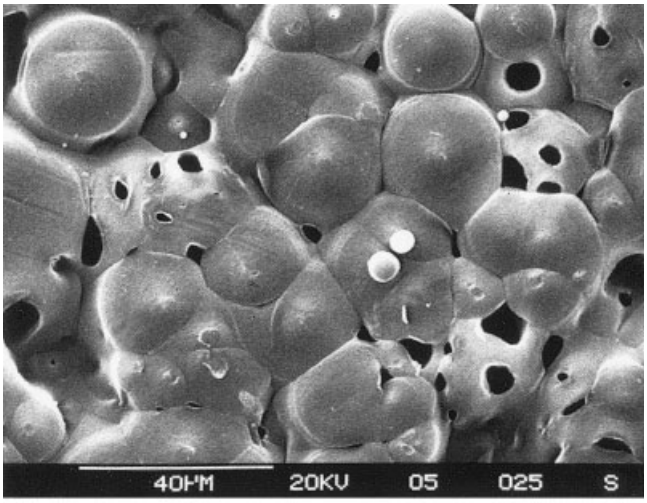

(a)

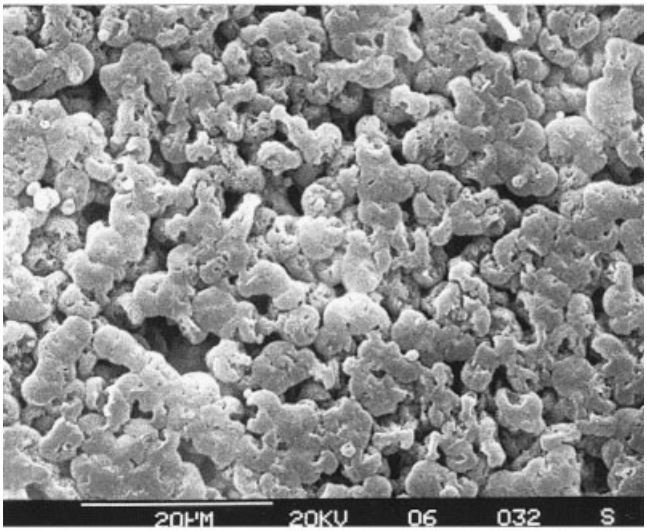

(b)

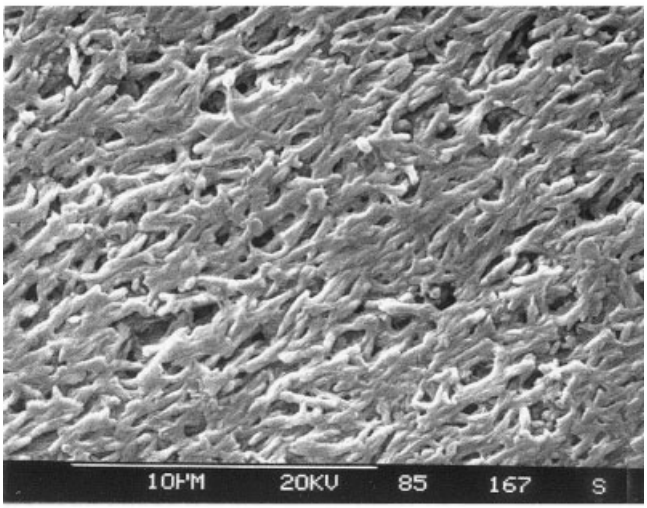

(c)

shape to those observed in the membrane cross section [Fig. 10(d)]. The nucleation density of crystalline particles here is very high as in the membrane bulk. The influence of a significant polymer-rich boundary layer at this top surface is not evident, apparently because of precipitation in a soft bath.

Bottom surfaces

The bottom surfaces of membranes AF, CF, and DF are shown in Figure 12(a–c). All the bottom surfaces of these membranes show evidence of both liquid–liquid phase separation and crystallization. As the water content in the dope is increased (from dope A to dope D), the rate of crystal nucleation is increased, and the resultant membrane has a higher density of crystallization particles. The bottom surface of membrane AF is shown in Figure 12(a). It has a truncated cellular structure initiated by liquid–liquid nucleation. As in case II, crystallization occurs after liquid–liquid phase separation. Unlike the closed cells in the membrane interior, the cellular voids in this bottom surface are not regular in terms of shape and size. There are many connections between the voids. This implies that the last stage of phase inversion [Fig. 1(d)] occurs to a significant extent on this bottom surface. The distortion of these pores is also enhanced by the crystallization that occurs some time during the phase inversion. This surface is, however, considered to be closed from the point of view of water permeability across the film (Table I) because the holes do not considerably penetrate the interior of the membrane. As crystallization becomes more dominant than liquid–liquid phase separation, the bottom surface opens as shown in membrane CF [Fig. 12(b)]. The open pores are surrounded by crystalline dumbbell-like or sheaflike particles (ca. 5 μm). Such an open structure is similar to the case III process discussed earlier, which occurs when crystallization and liquid–liquid phase separation occur on similar timescales. The particles on the bottom surface are flattened. This can be associated with crystal growth against the smooth glass plate. The morphology of the bottom surface of membrane DF is shown in Figure 12(c). The truncated cellular pores in the bottom surfaces of membranes AF and CF are hardly evident in this surface. The crystalline sticks that form on this surface have a structure intermediate between cases III and IV. The crystalline sticks are very small, and so they are not significantly flattened when they grow against the glass support.

Figure 11 SEM photomicrographs of the top surfaces of nylon 6 membranes prepared by the immersion of dopes A, C, and D in bath F: (a) membrane AF, (b) membrane CF, and (c) membrane DF.

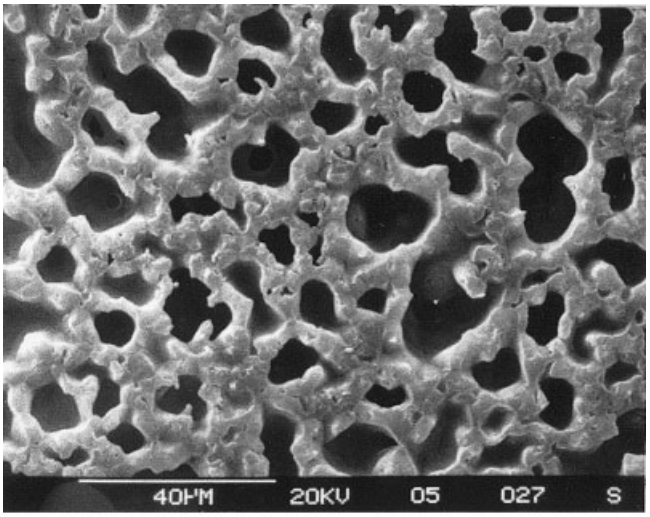

(a)

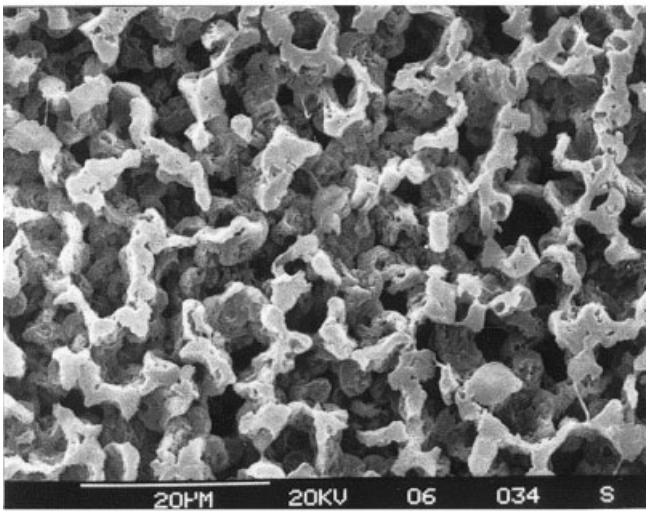

(b)

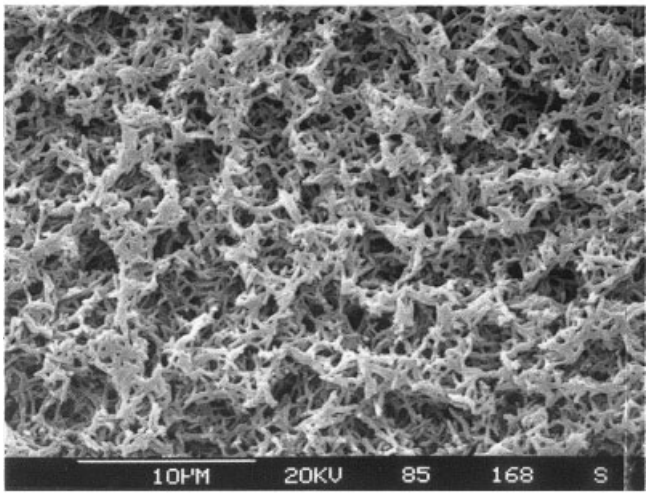

(c)

Figure 12 SEM photomicrographs of the bottom surface of nylon 6 membranes prepared by the immersion of dopes A, C, and D in bath F: (a) membrane AF, (b) membrane CF, and (c) membrane DF.

Effect of the bath on the membrane morphology

The solvent content of a bath is known to affect the relative rate of liquid–liquid phase separation and crystallization during precipitation.[25] With a soft bath that contains a large amount of solvent, liquid–liquid phase separation can be suppressed. Under this condition, the mass transfer of the solvent and nonsolvent across the membrane–bath interface is slow. The condition of a soft bath also favors the formation of a less concentrated gel layer near the top boundary region, which may easily be broken up to form an open surface during the crystallization process. On the contrary, if the bath is a pure nonsolvent, the equilibrium interfacial boundary condition will cause the formation of a dense skin boundary layer at the dope–bath interface. Because there is a strong driving force for mass transfer with a pure nonsolvent bath, the local composition will rapidly cross the binodal and make the local region supersaturated with respect to liquid–liquid phase separation and crystallization. Because of the higher surface energies involved in polymer crystallization, it is expected that under similar degrees of supersaturation, liquid–liquid nucleation will occur at a higher rate than polymer crystallization. For the nylon 6 system, these limiting bath conditions can be demonstrated by a comparison of membranes CF and CE. The structures of membrane CF are shown in Figures 10(b), 11(b), and 12(b), and those of membrane CE are shown in Figure 13(a–c). The cross section of membrane CE [Fig. 13(a)] shows the characteristics of liquid–liquid phase separation more strongly than the cross section of membrane CF [Fig. 10(b)]. The cellular structure typical of the amorphous terpolymer is more evident in membrane CE. There is little evidence of independent particles in this membrane cross section, whereas membrane CF has a high population of independent crystalline particles. The top surfaces of membranes CE and CF also show the trend of increasing crystallization influence. The top surface of membrane CE [Fig. 13(b)] is composed of polygonal grains that make this surface resist to fluid flow; yet the top surface of membrane CF [Fig. 11(b)] is open and composed of independent sheaf or circular particles that result from crystallization in a rather weak interfacial gel. The bottom surfaces of membranes CE [Fig. 13(c)] and CF [Fig. 12(b)] are similar, and they both show evidence of liquid–liquid phase separation and crystallization. The pores are open, and the crystalline particles are in the form of sheaves. The crystallization densities are also similar for membranes CE and CF.

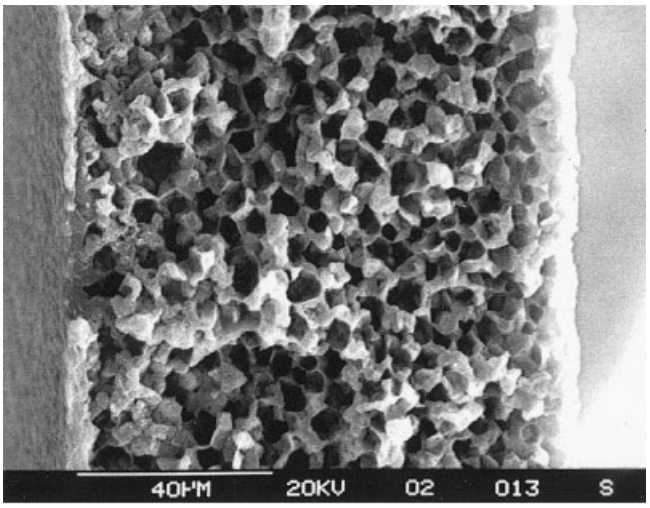

(a)

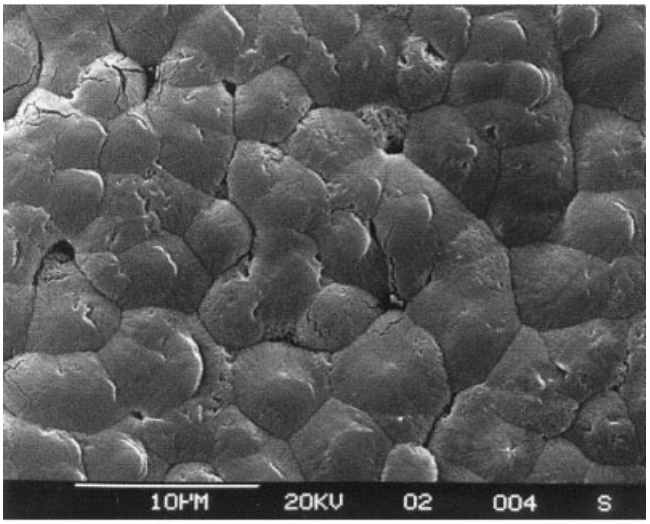

(b)

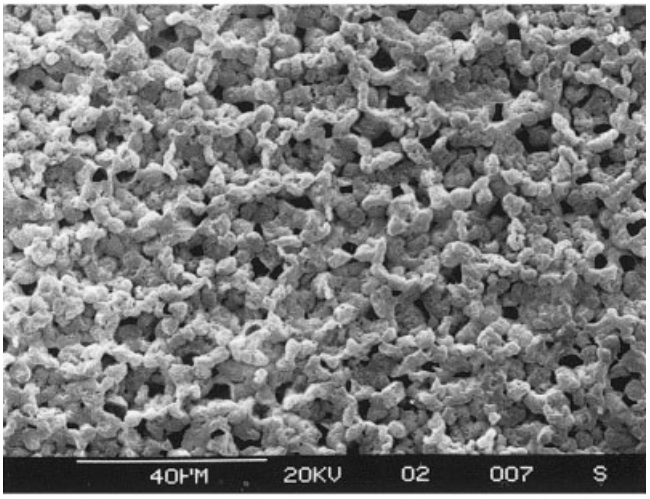

(c)

Figure 13 SEM photomicrographs of a nylon 6 membrane prepared by the immersion of dope C in bath E: (a) cross section, (b) top surface, and (c) bottom surface.

As the bottom of the membrane is far removed from the bath, it is thought that a sharp morphology difference attributed to bath characteristics will be less important in this surface.

CONCLUSIONS

The careful observation of the morphology of membranes precipitated from a water/formic acid/nylon 6 system provides many clues concerning the sequence of events that lead to precipitation. This system has potential for instability with respect to liquid–liquid phase separation and crystallization. These processes may occur sequentially or simultaneously, depending on the local driving forces. Under conditions in which the polyamide is dissolved in a good solution (polyamides may be protonated in formic acid solutions), crystal nucleation is slow, and liquid–liquid phase separation is expected to occur first and dominate the observed membrane morphology. If water is added to the dope solution, polyamide protonation is greatly reduced, and the polyamide coil begins to collapse as the solvent becomes weaker. Precipitation under these conditions occurs much more easily. If the bath is soft, crystallization is expected to be observed initially, and a particulate morphology will form, resulting in a skinless, microporous membrane. Skin formation is attributed to the buildup of high local polymer volume fractions in the boundary region contacting the bath. Skin formation is most dominant when the bath is harsh. It appears that the wettability of these structures is highly dependent on the microporosity and connectivity of the specific geometry of the precipitated nylon 6.

The authors thank Dee Breger of Columbia University Lamont Earth Observatory for the many hours of careful attention given to the preparation of the many scanning electron microscopy photomicrographs.

References

1. White, J. L.; Hancock, T. A. J Appl Polym Sci 1981, 26, 3157.
2. Couper, M. In High Technology Fibers; Leuin, M.; Preston, J., Eds.; Marcel Dekker: New York, 1985.
3. Kesting, R. E. Synthetic Polymeric Membranes; Wiley: New York, 1985.
4. Lovell, S. P.; Bush, J. H. U.S. Pat. 2,783,894 (1957).
5. Loeb, S.; Sourirajan, S. Adv Chem Ser 1962, 38, 117.
6. Smolders, C. A.; Reuver, A. J.; Boom, R. M.; Wienk, I. M. J Membr Sci 1992, 73, 259.
7. McKelvey, S. A.; Koros, W. L. J Membr Sci 1996, 112, 29.
8. Termonia, Y. J Membr Sci 1995, 104, 173.
9. Blaise, P. In Reverse Osmosis and Synthetic Membranes; Sourirajan, S., Ed.; National Research Council: Ottawa, Canada, 1977; Chapter 8.
10. Marinaccio, P. J.; Knight, R. A. U.S. Pat. 3,876,738 (1975).
11. Pall, D. B. U.S. Pat. 4,340,379 (1992).
12. (a) Knight, R. A. U.S. Pat. 5,084,179 (1993); (b) Knight, R. A. U.S. Pat. 5,264,165 (1993).

13. Bulte, A. M. W.; Folkers, B.; Mulders, M. H. V.; Smolders, C. A. J Appl Polym Sci 1993, 50, 13.
14. Grandine, R. U.S. Pat. 4,203,847 (1980).
15. Wienk, I. M.; Boom, R. M.; Beerlage, M. A. M.; Bulte, A. M. W.; Smolders, C. A. J Membr Sci 1996, 113, 361.
16. van de Witte, P.; Esselbrugge, H.; Dijkstra, P. J.; van den Berg, J. W. A.; Feijen, J. J Polym Sci Part B: Polym Phys 1996, 34, 2569.
17. Beltsios, K.; Steriotis, T.; Stefanopoulos, K.; Kanellopoulos, N. In Handbook of Porous Solids; Schueth, F.; Sing, K.; Weitkamp, J., Eds.; Wiley-VCH: Weinheim, 2002; Chapter 6.
18. Lin, D. J.; Beltsios, K.; Chang, C. L.; Cheng, L. P. J Polym Sci Part B: Polym Phys 2003, 41, 1578.
19. Lin, D. J.; Chang, C. L.; Huang, F. M.; Cheng, L. P. Polymer 2003, 44, 413.
20. Mulder, M. Basic Principles of Membrane Technology; Kluwer Academic: Dordrecht, 1991.
21. Cohen, C.; Tanny, G. B.; Prager, S. J Polym Sci Polym Phys Ed 1979, 17, 477.
22. Reuvers, A. J.; van den Berg, J. W. A.; Smolders, C. A. J Membr Sci 1987, 34, 45.
23. Reuvers, A. J.; Smolders, C. A. J Membr Sci 1987, 34, 67.
24. Tsay, C. S.; McHugh, A. J. J Polym Sci Part B: Polym Phys 1990, 28, 1327.
25. Cheng, L. P.; Dwan, A. W.; Gryte, C. C. J Polym Sci Part B: Polym Phys 1995, 33, 211.
26. Cheng, L. P.; Dwan, A. W.; Gryte, C. C. J Polym Sci Part B: Polym Phys 1995, 33, 223.
27. McHugh, A. J.; Miller, D. C. J Membr Sci 1995, 105, 121.
28. Paine, R. A. U. S. Pat. 3,408,315 (1968).
29. Nunes, S. P.; Inoue, T. J Membr Sci 1996, 111, 93.
30. Barth, C.; Goncalves, M. C.; Pires, A. T. N.; Roeder, J.; Wolf, B. A. J Membr Sci 2000, 169, 287.
31. Cahn, J. W.; Hilliard, J. E. J Chem Phys 1958, 28, 258.
32. Kim, J. Y.; Lee, H. K.; Kim, S. C. J Membr Sci 1999, 163, 159.
33. Beltsios, K.; Athanasiou, E.; Aidinis, C.; Kanellopoulos, N. J Macromol Sci Phys 1999, 38, 1.
34. Strathmann, H.; Kock, K.; Amar, P.; Baker, R. W. Desalination 1975, 16, 179.
35. Wijmans, J. G.; Baaij, J. P. B.; Smolders, C. A. J Membr Sci 1983, 14, 263.
36. Pinnau, I.; Koros, W. J. J Polym Sci Part B: Polym Phys 1993, 31, 419.
37. Wunderlich, B. Macromolecular Physics; Academic: New York, 1973; Vol. 1.
38. Young, T. H.; Lin, D. J.; Gau, J. J.; Chuang, W. Y.; Cheng, L. P. Polymer 1999, 40, 5011.
39. Brandrup, J.; Immergut, E. H. Polymer Handbook; Wiley: New York, 1966.
40. Kohan, M. I. Nylon Plastics; Wiley: New York, 1973.
41. Cheng, L. P.; Dwan, A. H.; Gryte, C. C. J Polym Sci Part B: Polym Phys 1994, 32, 1183.